Running Title: Characterizing Wsp1p-PRD

Interaction of the Proline-Rich Domain of Fission Yeast WASp (Ws1p1) with Actin Filaments

Aaron D. Rosenbloom[1] and Thomas D. Pollard[2]*

[1]Department of Chemistry, Yale University, PO Box 208107, New Haven, CT 06520-8103 USA

[2]Departments of Molecular Cellular and Developmental Biology, of Molecular Biophysics and Biochemistry and of Cell Biology
Yale University, PO Box 208103
New Haven, CT 06520-8103 USA

*Correspondence: thomas.pollard@yale.edu

Abstract

Background

The Wiskott-Aldrich Syndrome protein (WASp) family of proteins plays a crucial role in the activation of the Arp2/3 (actin-related protein 2/3) complex to promote the branching of actin filaments. The proline-rich domain (PRD) of WASp is known to contribute to branching nucleation but was overlooked, until experiments showed that the PRD of budding yeast Las17 can bind actin filaments (1).

Methods

We purified recombinant proline-rich domains from fission yeast *S. pombe* Wsp1 and budding yeast *S. cerevisiae* Las17 to test in biochemical assays of actin binding and polymerization.

Results

The PRD of the *S. pombe* Wsp1 binds actin filaments with micromolar affinity. The PRDs of both Wsp1 and Las17 slowed the rate of actin filament elongation by Mg-ATP-actin monomers by half and slowed the spontaneous polymerization of Mg-ATP-actin monomers modestly.

Conclusion

The affinity of PRDs of WASp-family proteins for actin filaments is high enough to contribute to the reported stimulation of actin filament branching by Arp2/3 complex.

Introduction

Actin, one of the most prevalent proteins in eukaryotes, assembles into filaments that support the physical integrity and contribute to movements of cells (2). Spontaneous nucleation of actin filaments is unfavorable (3), but formins and Arp2/3 complex nucleate filaments at times and places appropriate for cellular functions (4). Formins nucleate linear filaments such as those found in the cytokinetic contractile ring of a dividing cell, while Arp2/3 complex produces branched filaments at the leading edge of motile cells to produce movements.

Arp2/3 complex consists of seven protein subunits (5) responsible for the nucleation of branched filaments (6). The two actin related proteins (Arps) share the same fold as actin but have different surface characteristics (7). These Arps form a nucleus that allows for branched filament formation (8). However, the native Arp2/3 complex is intrinsically inactive, owing to Arp2 and Arp3 being separated from each other, precluding the formation of the nucleus needed

for actin polymerization (7). Proteins called nucleation-promoting factors (NPFs) and binding to the side of an actin filament activate Arp2/3 complex to form branches (9).

Nucleation promoting factors such as the Wiskott-Aldrich Syndrome protein (WASp) family have C-terminal motifs (10) including one or two verprolin-homology motifs (V) that bind actin monomers and central (C) and acidic (A) motifs that bind Arp2/3 complex (11). In addition to these VCA motifs, many NPFs have a proline-rich domain (PRD) before the VCA motif (12). The domains between the N-terminus and the PRD differ among the NPFs and contribute to regulation (12).

Studies of Arp2/3 complex activation by NPFs have focused on the VCA motif (13-15) but other evidence shows that the PRD plays a role in Arp2/3 complex activation (1, 9, 12, 16). First, the NPF activity of Scar, WASP, and Las17 are higher for constructs that include the PRD in addition to the VCA motif (9, 16, 17). Second, defects in endocytosis by budding yeast cells are more severe when both VCA and the PRD are removed from Las17, its WASp homolog (12). Third, the PRD of budding yeast Las17 was reported to stimulate the nucleation of actin filaments (1).

This evidence points to a role for the PRD in the activation of Arp2/3 complex, beyond its interaction with the SH3 domains of proteins that activate WASp and related proteins (18). However, much remained to be learned about the quantitative aspects of the molecular mechanisms. The work on Las17 opened a window into the role of the PRD, but other model organisms had not been tested. One such model organism is *S. pombe*.

S. pombe is a highly studied fission yeast (19) that has been used extensively to study endocytosis (20), a process driven by actin filament branching by Arp2/3 complex (21). Wsp1p is the WASp homologue of *S. pombe* (22). We measured affinity of Wsp1p-PRD for actin filaments and tested its effects on actin polymerization. We find that the PRD region binds actin filaments with micromolar affinity and slows the elongation of actin filaments by Mg-ATP-actin monomers.

Methods and Materials

Plasmid preparation

The DNA encoding amino acids 229 – 490 of *S. pombe* Wsp1p was amplified from genomic DNA and inserted into the pGEX-6P vector via In-Fusion cloning (Takara Bio USA). This

vector added an N-terminal GST tag with a precision protease recognition site. After cleavage at this site, the vector leaves 5 amino acids on the N-terminus of the protein. The last of these five is amino acid 228, so the final protein includes amino acids 228-490. Six histidine residues were added to the C-terminus of the sequence via the Q5 Site-Directed Mutagenesis Kit (New England Biolabs). The resulting vector was transformed into OverExpress C41(DE3) chemically competent *E. coli* cells (Lucigen). To allow for fluorescent labeling of Wsp1p-PRD, a cysteine was added to the N-terminus of the coding sequence directly after the precision protease recognition site or after the six-histidine tag on the C-terminus using the Q5 Site-Directed Mutagenesis Kit (New England Biolabs).

A plasmid encoding amino acids 301-536 of *S. cerevisiae* Las17 in a pGEX-6P vector was a generous gift from the laboratory of Kathryn Ayscough at the University of Sheffield. This plasmid attaches a GST-tag to the N-terminus of Las17-PRD. When cleaved by lab made Precision Protease, five amino acids are left at the N-terminus of the PRD.

Protein Expression and Purification

Transformed *E. coli* were grown in flasks with 1 L of LB-ampicillin at 37 °C with shaking at 200 RPM. When the optical density at 595 nm reached 0.4 – 0.5, we added 100 µL of 1 M isopropyl ß-D-1-thiogalactopyranoside (IPTG) and incubated overnight at 18 °C with shaking at 250 RPM. The cells were harvested by centrifugation at 5,000 g for 15 min. Bacterial pellets from 4 L of cell culture were resuspended in 165 mL of lysis buffer at pH 7.4 (480 mM NaCl, 3 mM KCl, 10 mM phosphate, 10 mM imidazole, 1 mM PMSF, and an inhibitor cocktail that gave final concentrations of 1 µg/mL of bestatin, aprotinin, leupeptin, and pepstatin). The resuspended cells were frozen and stored at -20 °C until use.

Resuspended pellets of cells from 4 L of culture were thawed in a room temperature water bath and sonicated on ice 8 times for 1 min with one-minute rest intervals using a 3/8 inch probe at 50% duty cycle and an output control of 6 on a Branson Sonifier 450. The lysate was clarified by centrifugation in a Type 45 Ti rotor (Beckman Coulter) at 35,000 RPM for 35 min at 4 °C. The supernatant stirred with 10 mL of TALON metal affinity resin (Takara Bio US) equilibrated in Buffer A (480 mM NaCl, 3 mM KCl, 10 mM phosphate, and 10 mM imidazole, pH 7.4) for 1 h at 4 °C. The resin was pelleted and washed three times with 40-45 mL of cold wash buffer. Bound protein was eluted from the washed resin four times for at least 10 min with

10 mL of cold elution buffer at a pH of 7.4 (Buffer A with an additional 240 mM imidazole) followed by pelleting after each elution. The combined eluants were incubated overnight at 4 °C with 5 mL of Glutathione-Sepharose 4B resin (GE Healthcare Bio-sciences AB). The beads were placed in a column and washed 3 times with 50 mL of Buffer B (480 mM NaCl, 3 mM KCl, and 10 mM phosphate, pH 7.4) and three times with 50 mL of KMEID buffer (50 mM KCl, 1 mM $MgCl_2$, 1 mM EGTA, 10 mM imidazole pH 7.0, 2 mM DTT). The beads were suspended in 5 mL of KMEID and the protein was cleaved overnight at 4 °C using ~0.2 mg of lab made GST tagged Precision Protease. The cleaved protein was collected from the column and concentrated approximately 10-fold using an Amicon Ultra Centrifugal Filter Unit (Millipore) with a 3,000 Da cutoff. The concentrated protein was dialyzed two times against 500-1,000 mL KMEI buffer.

For labeling with Alexa488, Wsp1p-PRD and Wsp1p-PRD were purified up to the first set of washes of the Glutathione-Sepharose 4B resin. The beads were then washed with 5 mL of KMIT (50 mM KCl, 1 mM $MgCl_2$, 10 mM imidazole pH 7.0, 2 mM tris(2-carboxyethyl)phosphine, TCEP) and the protein was cleaved with lab made GST tagged Precision Protease as above. The cleaved protein was labeled by introducing 500 nmole Alexa Fluor 488 maleimide (Thermo Fisher Scientific) to the cleaved solution and incubating at 4 °C overnight. The conjugated protein was incubated with 200 µL of equilibrated TALON resin for one hour. The beads were pelleted and washed 3 times with 1 mL of KMIT buffer. The protein was eluted with 5 sets of 200 µL KMI+ (50 mM KCl, 1 mM $MgCl_2$, 250 mM imidazole pH 7.0). The protein was dialyzed against two changes of 500 mL of KMEI and concentrated using an Amicon Ultra Centrifugal Filter Unit (MilliporeSigma) with a 3,000 Da cutoff. The concentration of the dye conjugated to the protein was determined by absorption at 495 nm with an extinction coefficient of 71,000 M^{-1} cm^{-1}.

Las17-PRD was expressed in OverExpress C41(DE3) *E. coli* cells (Lucigen) and purified as described by Urbanek *et al*. (1) with minor modifications. One-liter cultures of TB-ampicillin were incubated at 37 °C with shaking at 200 RPM until an optical density at 595 nm of approximately 0.4 – 0.5. Then each flask was induced with 1 mL of 1 M IPTG overnight at 37 °C with shaking at 250 RPM. Cell pellets were resuspended in 40 mL of modified lysis buffer (10 mM phosphate buffer pH 7.4, 480 mM NaCl, 3 mM KCl, 1 mM PMSF, and an inhibitor cocktail that gave final concentrations of 1 µg/mL of bestatin, aprotinin, leupeptin, and pepstatin) per 4 L of culture. The resuspended cells were frozen and stored at -20 °C until use.

Pellets from 4 L of culture were thawed at room temperature, sonicated on ice and clarified as above. The supernatant was added to 5 mL of equilibrated Glutathione Sepharose 4B resin (GE Healthcare Bio-sciences AB). The beads were washed in a column 3 times with 50 mL of Buffer C (10 mM phosphate buffer pH 7.4, 480 mM NaCl, 3 mM KCl, and 0.1% Tween-20), three times with 50 mL of Buffer D (10 mM phosphate buffer pH 7.4, 140 mM NaCl, and 3 mM KCl), two times with 50 mL of Buffer E (50 mM Tris-HCl, 400 mM NaCl, 1 mM EDTA, 1 mM DTT, pH 7) and two times with 50 mL of Buffer F (50 mM Tris-HCl, 150 mM NaCl, 1 mM EDTA, 1 mM DTT, pH 7). The beads were placed in 5 mL of Buffer F and the protein was cleaved overnight at 4 °C using ~0.2 mg of lab made GST tagged Precision Protease. The cleaved protein was removed from the column, concentrated, and dialyzed two times against 500 – 1,000 mL of KMEI buffer as above.

Actin purification and labeling

Actin was isolated from an acetone powder of chicken breast muscle and purified by one cycle of polymerization, pelleting, and depolymerization before gel filtration chromatography on a Sephacryl-S300 column in G-buffer (23). For labeling, actin filaments at a concentration of 1 mg/mL in 0.1 M KCl, 2 mM $MgSO_4$, 25 mM Tris pH 7.5, 3 mM NaN_3, and 0.3 mM ATP were reacted with a 10-fold molar excess of *N*-(1-pyrene)iodoacetamide (Thermo Fisher Scientific) dissolved in dimethylformamide (DMF) at 4 °C overnight. The actin filaments were pelleted, homogenized in G-buffer, depolymerized by dialysis against G-buffer for two days at 4°C, and clarified at 75,000 RPM in a TLA 120.2 rotor (Beckman Coulter) at 4 °C for 2 h. The upper two thirds of the supernatant were gel filtered on a Superdex-200 column in G-buffer.

Mass spectrometry

A sample of the purified protein was run on a Mini-PROTEAN TGX Stain-free gel (BIORAD) with 4-20% acrylamide gradient and stained with Coomassie brilliant blue. The stained bands were cut out of the gel. The Mass Spectrometry and Proteomics Resource of the W. M. Keck Foundation Biotechnology Resource Laboratory of Yale University digested the bands with trypsin and analyzed the peptides by MS/MS mass spectrometry.

166 Concentration determination

167 The concentrations of samples of Wsp1p-PRD and Las17-PRD were determined by SDS-PAGE,
168 staining with Coomassie brilliant blue and densitometry with a range of amounts of chicken
169 skeletal muscle actin as the standard. Samples were run on a 15-well Mini-PROTEAN TGX
170 Stain-free gel (BIORAD) with 4-20% polyacrylamide gradient. Gels were stained with
171 Coomassie blue, destained 3 times for 10 min with 25% methanol and 10% acetic acid, and
172 soaked in water overnight. Gels were imaged with a ChemiDoc Imaging System (BIORAD). The
173 densities of the bands were determined with ImageJ software. The mass of the PRD sample was
174 determined by comparison with the linear standard curve. A molar concentration of the protein
175 was calculated using molecular weights of 26.7 kD for Wsp1p-PRD and 24.6 kD for Las17-
176 PRD.

177

178 Actin filament binding assay

179 A high concentration of actin monomers was polymerized in KMEI buffer and used to prepare
180 100 µL samples with 0, 2.5, 5, 10, 25, 50, 100, and 180 µM actin and 1 µM of Alexa488-Wsp1p-
181 PRD or Wsp1p-PRD-Alexa488. Samples were centrifuged in a TLA 100 rotor (Beckman
182 Coulter) at 75,000 RPM for 30 min. The fluorescence of 75 µL of supernatant was measured
183 with a Gemini EM microplate reader (Molecular Devices) with excitation at 495 nm and
184 emission at 519 nm with a cutoff at 515 nm with 6 flashes per read. The plate was turned 180
185 degrees and re-measured to be certain there was no instrumental bias in the measurements.

186 The fluorescence of the supernatants of the 50 µM, 100 µM, and 180 µM actin samples
187 were averaged and used to correct for background fluorescence. The corrected fluorescence
188 measurements of the 0 µM actin samples were averaged to determine the value of unbound
189 protein. Subtracting the ratio of each corrected fluorescence value to the average fluorescence
190 value of 100% unbound protein from 1 gave the fraction of bound protein. The fraction of bound
191 protein was plotted against the concentration of actin. The dissociation equilibrium constant (K_d)
192 was determined by fitting

193 $$\text{fraction bound} =$$

194 $$\frac{([\text{Actin}] + \{\text{Wsp1p} - \text{PRD}]_{\text{total}} + K_d) - \sqrt{([\text{Actin}] + \{\text{Wsp1p} - \text{PRD}]_{\text{total}} + K_d)^2 - 4[\text{Actin}]\{\text{Wsp1p} - \text{PRD}]_{\text{total}}}}{2\{\text{Wsp1p} - \text{PRD}]_{\text{total}}}$$ to

195 the data.

196

Fluorescence anisotropy experiments

Concentrations of 20 nM Alexa488-Wsp1p-PRD or 100 nM Wsp1p-PRD-Alexa488 were incubated in KMEI buffer at room temperature for 30 min with 0, 2.5, 5 or 10 μM filamentous actin. Anisotropy was measured with an Alpha-scan spectrofluorometer (Photon Technology International) with excitation at 495 nm and emission of 519 nm. The excitation bandpass was set to 4 nm and the emission bandpass was at 20 nm. Each sample was measured at four different settings: first (HV), excitation polarizer at 90° and the emission at 90°; second (HH), excitation at 90° and emission at 0°; third (VV), excitation at 0° and emission at 0°; and fourth (VH), excitation polarizer at 0° and emission at 90°. Emission measurements were taken every second for 10 s. For Alexa488-Wsp1p-PRD 5 replicates were collected for 2.5, 5, and 10 μM polymerized actin, and a total of 6 replicates for 0 μM filamentous actin. For Wsp1p-PRD-Alexa488, only one sample was measured for each concentration.

To calculate the anisotropy of each sample, the 10 measurements of HH, HV, VV, and VH were averaged for each sample. The G-factor for each sample was calculated according to $G = \frac{HV}{HH}$. All the calculated G-factors were averaged together to determine the final G-factor. The anisotropy was calculated according to the formula $anisotropy = \frac{VV - G(VH)}{VV + 2G(VH)}$.

Assay for the polymerization of bulk samples of actin

Pyrene-labeled (10%) Ca-ATP-actin monomers were exchanged for Mg^{2+} by adding 10x MEA buffer resulting in 50 μM $MgCl_2$, 200 μM EGTA pH 8.0, 0.00005% Antifoam 204 (Sigma) and incubating at room temperature for 2-5 min. Polymerization was initiated by mixing two volumes of PRD in 1.5x of KMEIA buffer (1x: 50 mM KCl, 1 mM $MgCl_2$, 1 mM EGTA, 10 mM imidazole pH 7.0, 0.00005% Antifoam 204) or KMEIA alone with the Mg-ATP-actin monomers. The time course of the fluorescence change was measured with a SpectraMax Gemini EM Microplate Reader (Molecular Devices) with excitation at 365 nm and emission at 407 nm in a Costar 3694 EIA/RIA, 96 well, half area, flat bottom, non-treated, black polystyrene plates using one flash per read every 2 min for 1 μM and 2.5 μM actin, every 10 s for 5 μM and 7.5 μM actin, and every 5 s for 10 μM actin. Since the 1 μM and 2.5 μM samples were run overnight, an optical adhesive was placed on top to prevent evaporation.

The data was processed by adding the deadtime and normalized similar to Doolittle *et al.* (24) for the initial minimum (I_{min}) and final maximum (I_{max}) values. Fluorescence intensities were converted to the polymerized actin concentration by first subtracting the I_{min} from each intensity and taking into account the critical concentration of 0.1 µM.

Measurement of elongation rates

Samples of 150 µL in wells of Costar 3694 EIA/RIA polystyrene plates consisted of 2 µM Mg-ATP-actin monomers, 0.5 µM pre-polymerized actin filament seeds, and either no PRD, 7.5 µM Wsp1p-PRD or 7.5 µM Las17-PRD in 50 mM KCl, 1 mM $MgCl_2$, 1 mM EGTA, 10 mM imidazole pH 7.0, 0.00005% Antifoam 204. Fluorescence was measured every 5 s with a SpectraMax Gemini EM Microplate Reader (Molecular Devices) with excitation at 365 nm and emission at 407 nm. The dead time between adding actin monomers and acquisition was noted.

The data was processed similar to the spontaneous polymerization data. To correct for the photobleaching, the intensities after T_{max} for the no PRD samples were fit to an exponential. The exponentials for all the samples without PRD were averaged together (n = 6) and used to correct for photobleaching. The samples without PRD were used to determine I_{min} and I_{max} for all samples. We calculated the number concentration of filaments for the reactions without PRD from the rate of elongation and the rate constant for elongation (25). To calculate the barbed-end elongation rates for each of the reactions, we divided the average rate of polymerization of each set of samples in µM s^{-1} by the concentration of filament ends. We measured a total of six replicates without PRD, four replicates for Wsp1p-PRD, and three replicates for Las17-PRD.

Results

Attempts to purify Wsp1p-PRD with just a GST tag at the N-terminus produced many protein fragments, likely due to ribosome stalling on polyproline sequences (26) and producing truncated proteins. To eliminate these fragments, we appended a 6x-histidine tag to the C-terminus of GST-Wsp1p-PRD. After two affinity purification steps, Wsp1p-PRD ran as the largest band on SDS-PAGE with only slight contamination (Fig. 1). Mass spectrometry of a trypsin digest of the major band confirmed it is Wsp1p-PRD. The Wsp1p-PRD band ran slower than expected from its molecular weight of 26.7 kD (Fig. 1), similar to other proline-rich proteins (27). We also purified Las17-PRD by small modifications of the method of Urbanek *et al*. (1) (Fig. 2). Mass

spectrometry of a trypsin digest identified the dominant band as Las17-PRD, the higher molecular weight contaminant as the *E. coli* chaperonin dnaK and the minor lower molecular weight bands as fragments of Las17-PRD, likely produced by ribosomal stalling.

Fig. 1. SDS-PAGE and Coomassie brilliant blue staining of samples from each step of the purification of Wsp1p-PRD. Left gel: lane 1, protein standards; lane 2, crude lysate; lane 3 clarified sample of crude lysate applied to TALON resin; lane 4, unbound flowthrough from TALON resin; lanes 5-7, successive washes of TALON resin with Buffer A (480 mM NaCl, 3 mM KCl, 10 mM phosphate, 10 mM imidazole pH 7.4); lanes 8-11, elution of bound proteins from TALON resin with elution buffer (Buffer A with an additional 240 mM imidazole pH 7.4). Right gel: lane 1, protein standards; lane 2, combined fractions eluted from TALON resin and applied to glutathione Sepharose 4B beads; lane 3, unbound flowthrough from glutathione Sepharose 4B beads; lanes 4-6, successive washes of the glutathione Sepharose 4B beads with Buffer B (480 mM NaCl, 3 mM KCl, and 10 mM phosphate at a pH 7.4); lanes 7-9, washes of glutathione Sepharose 4B beads with KMEID (50 mM KCl, 1 mM $MgCl_2$, 1 mM EGTA, 10 mM imidazole pH 7.0, 2 mM DTT); lane 10, pure Wsp1p-PRD cleaved from glutathione Sepharose 4B beads. The arrowhead marks Wsp1p-PRD.

Fig. 2. Coomassie brilliant blue stained SDS-PAGE gel of purification steps of *S. cerevisiae* Las17-PRD. Lane 1, protein standards; lane 2, crude lysate; lane 3, clarified lysate applied to glutathione Sepharose 4B beads; lane 4, unbound flowthrough from glutathione Sepharose 4B beads; lanes 5-7, washes of glutathione Sepharose 4B beads with Buffer C (10 mM phosphate buffer pH 7.4, 480 mM NaCl, 3 mM KCl, and 0.1% Tween-20); lanes 8-10, washes of glutathione Sepharose 4B beads with Buffer D (10 mM phosphate buffer pH 7.4, 140 mM NaCl, and 3 mM KCl); lanes 11-12, washes of glutathione Sepharose 4B beads with Buffer E (50 mM Tris-HCl, 400 mM NaCl, 1 mM EDTA, 1 mM DTT, and brought to a pH of 7 at room temperature); lanes 13-14, washes of glutathione Sepharose 4B beads with Buffer F (50 mM Tris-HCl, 150 mM NaCl, 1 mM EDTA, 1 mM DTT brought to pH 7 at room temperature); lane 15, protein cleaved from glutathione Sepharose 4B beads. Mass spectrometry of tryptic digests identified the main band (arrowhead) as Las17-PRD, the upper band as *E. coli* dnaK, and the

minor lower molecular weight bands as fragments of Las17-PRD, likely due to ribosome stalling.

PRDs have no aromatic residues to measure absorbance at 280 nm; therefore, we estimated their concentrations by densitometry of Coomassie brilliant blue stained Wsp1p-PRD bands run on SDS-PAGE compared with a standard curve of known amounts of actin. This measurement is not the ideal, as proteins may stain differently in Coomassie blue (28, 29).

We determined the binding affinity of fluorescently labeled Wsp1p-PRD for actin filaments by measuring the fraction of 1 μM N-terminally (Alexa488-Wsp1p-PRD) or C-terminally (Wsp1p-PRD-Alexa488) labeled Wsp1p-PRD that pelleted with a range of actin filament concentrations from 0 – 180 μM (Fig. 3A and B). We calculated the fraction bound by measuring the fluorescence of unbound Wsp1p-PRD in the supernatants. Fitting a binding isotherm to the data gave a K_d of 6.2 ± 0.6 μM for Alexa488-Wsp1p-PRD (Fig. 3A). We confirmed that the N-terminal fluorescent tag does not affect binding by measuring the fraction for C-terminally (Wsp1p-PRD-Alexa488) labeled Wsp1p-PRD that pelleted with a range of actin filament concentrations (Fig. 3B). The K_d of 5 ± 1 μM for Wsp1p-PRD-Alexa488 was similar to Alexa488-Wsp1pPRD.

Fig. 3. Affinity of labeled Wsp1p-PRD for actin filaments determined by cosedimentation and fluorescence anisotropy. (A-B) A range of concentrations of actin filaments were incubated with 1 μM of Alexa-488 labeled Wsp1p-PRD in 50 mM KCl, 1 mM $MgCl_2$, 1 mM EGTA, 10 mM imidazole at pH 7.0 for 30 min at 25°C followed by ultracentrifugation at 240,000 g for 30 min. The fraction bound was calculated from the fluorescence of the supernatant. (A) Fraction of Alexa488-Wsp1p-PRD bound vs. actin filament concentration. Points are the mean with standard deviation as the error (n = 5-6). The solid line is the fit to the data of a binding isotherm with a K_d of 6.1 ± 0.6 μM .(B) Fraction of Wsp1p-PRD-Alexa488 bound vs. actin filament concentration. Points are the mean with the range as the error (n = 2-3). The solid line is the fit to the data of a binding isotherm with a K_d of 3 ± 1 μM. (C-D) A range of concentrations of actin filaments were incubated with 20 nM of Alexa488-Wsp1p-PRD or 100 nM of Wsp1p-PRD-Alexa 488 in 50 mM KCl, 1 mM $MgCl_2$, 1 mM EGTA, and 10 mM imidazole at pH 7.0 at 25°C. Each sample was excited with polarized light, and the anisotropy was calculated based on the

polarized components of the emission. (C) Fluorescence anisotropy of Alexa488-Wsp1p-PRD vs. concentration of actin filaments. Points are the mean ± standard deviation (n = 5-6). (D) Fluorescence anisotropy of Wsp1p-PRD-Alexa488 vs. concentration of actin filaments. Points are values from one experiment.

We used similar samples to measure the effects of actin filaments on the fluorescence anisotropy of the N- and C-terminally tagged Wsp1p-PRD. Surprisingly, actin filaments did not change the anisotropy in spite of binding the tagged Wsp1p-PRD (Fig. 3C and D). Therefore, binding to actin filaments did not change the rotational diffusion of Alexa-488 at either end of Wsp1p-PRD.

The presence of 5 μM Wsp1p-PRD or Las17-PRD slowed the time course of spontaneous polymerization of 5 μM Mg-ATP actin monomers modestly (Fig. 4A). This is the opposite to the previous reports for 0.08-0.14 μM Las17-PRD with 5 μM rabbit muscle Ca-ATP-actin in polymerization buffer with $MgCl_2$ and EGTA at pH 8.0 (1, 30).

Fig. 4. Effects of PRDs on the time course of the spontaneous polymerization of 5 μM of Mg-ATP-actin monomers (10% pyrenyl-actin). Conditions: 50 mM KCl, 1 mM $MgCl_2$, 1 mM EGTA, 10 mM imidazole pH 7.0, 0.6 mM Tris, 0.15 mM DTT, 60 μM ATP, 30 μM $CaCl_2$ and 0.00005% Antifoam 204 in the presence of two concentrations of (A) Wsp1p-PRD or (B) Las17-PRD.

To understand how the PRD slows spontaneous polymerization, we used the fluorescence of pyrenyl-actin to measure the elongation rates of actin filament seeds in the presence of PRD. The polymerization samples contained 2 μM Mg-ATP-actin (10% labeled with pyrene), 0.5 μM of polymerized actin to provide seeds, and either no PRD, 5 μM Wsp1p-PRD, or 5 μM Las17-PRD (Fig. 5A). The fluorescence increased linearly between 50 and 120 s (Fig. 5B) characteristic of pure elongation without a contribution from spontaneous nucleation (31). Polymerization of 2.5 μM Mg-ATP-pyrenyl-actin monomers without filament seeds started with a clear lag (Fig. 5A). Thus, under the conditions used, little spontaneous nucleation occurred during the first 120 s of the reaction, so all of the polymerization during this time came from elongation of previously formed filament seeds.

Fig. 5. Effect of PRDs on the time course of elongation of actin filaments from preformed seeds (0.5 µm polymerized actin, 0.3 nM ends). Conditions: 2 µM 10% Mg-ATP-pyrenyl-actin monomers with either no PRD (black), 5 µM Wsp1p-PRD (green), or 5 µM of Las17-PRD (pink). For comparison, 2.5 µM of 10% Mg-ATP-pyrenyl-actin with the equivalent amount of labeled actin were polymerized without preformed filaments or PRD (grey). (A) Examples of time courses corrected for photobleaching. (B) Initial parts of the polymerization curves from A after the initial dead time.

Since the rate constants for actin filament elongations are known (25) we used the samples without PRD to calculate that the concentration of filament ends added to each reaction was 300 ± 100 pM (average concentration ± standard deviation; n = 6). The rate of barbed end elongation of samples of 2 µM actin monomers was 20 ± 10 subunits s^{-1} without PRD; n = 6 for rate), 10 ± 4 subunits s^{-1} with 5 µM of Wsp1p-PRD (same as above; n = 4 for rate), and 9 ± 3 nM s^{-1} with 5 µM of Las17-PRD (same as above; n = 3 for rate). Therefore, both Wsp1p-PRD and Las17-PRD reduced the elongation rate by approximately half.

Discussion

Binding affinity: Previous work (1) presented evidence that the PRD of Wsp1p family proteins can bind actin filaments but did not measure the affinity of the interaction with standard methods. The methods used included two-hybrid assays, pelleting with single concentrations of PRD, and actin and polymerization time courses. Urbanek *et al. (1)* estimated the affinity for actin filaments to be 0.22 µM from a double reciprocal plot of 1/actin polymerization rate vs. 1/[Las17 PRD] (their Fig. S2), but <20% of 5 µM PRD pelleted with 5 µM actin filaments corresponding to a K_d of about 20 µM (their Fig. 1D). Microscale thermophoresis was also used to measure a K_d of 24 nM for the 300–422 fragment of Las17 binding to actin monomers (1, 30).

Our quantitative binding assays confirmed that the Wsp1-PRD binds muscle actin filaments with micromolar affinity using Wsp1-PRD labeled on either end with Alexa-488. Surprisingly, even when most of the Wsp1-PRD was bound to the filaments, the Alexa-488 on both ends of the PRD remained mobile. This is consistent with binding being mediated by the

379 middle of the PRD as shown for Las17-PRD (1, 30) and the known flexibility of peptides with
380 disordered links between proline-rich sequences (32).
381 *Effects on polymerization:* Urbanek *et al.* (1) reported that submicromolar concentrations
382 of Las17 PRD stimulate spontaneous polymerization of 5 µM Ca-ATP-actin monomers in buffer
383 with $MgCl_2$ (conditions where the exchange of bound Ca^{2+} for Mg^{2+} is rate limiting), consistent
384 with promoting nucleation but also with an effect on divalent cation exchange. They also
385 reported that submicromolar concentrations of Las17-PRD increased the steady-state
386 fluorescence of pyrenyl-actin filaments, which they interpreted as a decrease in the critical
387 concentration. However, a substantial change in the polymer concentration under their conditions
388 without PRD would have been unlikely, since the polymer concentration would have been 4.9
389 µM and the monomer concentrations 0.1 µM, an already low concentration.
390 We found that 5 µM concentrations of either Wsp1p-PRD or Las17-PRD slow the time
391 course of spontaneous polymerization of 5 µM Mg-ATP-actin monomers, while 2.5 µM Las17-
392 PRD had less effect on spontaneous polymerization. Both Las17-PRD and Wsp1p-PRD slowed
393 the elongation of actin filament barbed ends by about half. This is a plausible explanation for the
394 inhibition of spontaneous polymerization; however, more work is necessary to fully understand
395 the mechanism of inhibition. This new finding raises the possibility that the effect of Las17-PRD
396 on the polymerization of Ca-ATP-actin in buffer containing $MgCl_2$ (1) may have been due to
397 increasing the rate limiting exchange of Mg^{2+} for Ca^{2+} rather than effect on the polymerization
398 reaction.
399 The micromolar affinity of Wsp1p-PRD for actin filaments has interesting implications
400 for its function. As the total concentration of actin in the fission yeast cell is >50 µM and much
401 higher than this average in endocytic actin patches (33), it stands to reason that a substantial
402 fraction of Wsp1 is bound to actin filaments inside cells, especially at sites where branched actin
403 filaments form. Given the mobility of both ends of the PRD bound to an actin filament revealed
404 by fluorescence anisotropy (Fig. 3C and D), the VCA region of a Wsp1 molecule bound by its
405 PRD to an actin filament should be capable of binding and activating Arp2/3 complex to
406 nucleate an actin filament branch on a mother filament. On the other hand, the 4 µM
407 concentration of Wsp1 in the cytoplasm of fission yeast (34) will likely have a only a small
408 effect on the growth of the much higher concentration of actin filaments.
409

Acknowledgements

Research reported in this publication was supported by National Institute of General Medical Sciences of the National Institutes of Health under award number R01GM026338. The content is solely the responsibility of the authors and does not necessarily represent the official views of the National Institutes of Health. The authors thank the laboratory of Kathryn Ayscough at the University of Sheffield for providing the plasmid for Las17-PRD and advice about its purification.

Competing interests: The authors declare that no competing interests exist.

References

1. Urbanek AN, Smith AP, Allwood EG, Booth WI, Ayscough KR. A novel actin-binding motif in Las17/WASP nucleates actin filaments independently of Arp2/3. Curr Biol. 2013;23(3):196-203.

2. Pollard TD, Cooper JA. Actin, a central player in cell shape and movement. Science. 2009;326(5957):1208-12.

3. Rosenbloom AD, Kovar EW, Kovar DR, Loew LM, Pollard TD. Mechanism of actin filament nucleation. Biophys J. 2021;120(20):4399-417.

4. Pollard TD. Regulation of actin filament assembly by Arp2/3 complex and formins. Annu Rev Biophys Biomol Struct. 2007;36:451-77.

5. Machesky LM, Atkinson SJ, Ampe C, Vandekerckhove J, Pollard TD. Purification of a Cortical Complex Containing 2 Unconventional Actins from Acanthamoeba by Affinity-Chromatography on Profilin-Agarose. J Cell Biol. 1994;127(1):107-15.

6. Mullins RD, Heuser JA, Pollard TD. The interaction of Arp2/3 complex with actin: Nucleation, high affinity pointed end capping, and formation of branching networks of filaments. Proc Natl Acad Sci U S A. 1998;95(11):6181-6.

7. Robinson RC, Turbedsky K, Kaiser DA, Marchand JB, Higgs HN, Choe S, et al. Crystal structure of Arp2/3 complex. Science. 2001;294(5547):1679-84.

8. Rouiller I, Xu XP, Amann KJ, Egile C, Nickell S, Nicastro D, et al. The structural basis of actin filament branching by the Arp2/3 complex. J Cell Biol. 2008;180(5):887-95.

9. Machesky LM, Mullins RD, Higgs HN, Kaiser DA, Blanchoin L, May RC, et al. Scar, a WASp-related protein, activates nucleation of actin filaments by the Arp2/3 complex. Proc Natl Acad Sci U S A. 1999;96(7):3739-44.

10. Kurisu S, Takenawa T. The WASP and WAVE family proteins. Genome Biol. 2009;10(6).

11. Marchand JB, Kaiser DA, Pollard TD, Higgs HN. Interaction of WASP/Scar proteins with actin and vertebrate Arp2/3 complex. Nat Cell Biol. 2001;3(1):76-82.

12. Tyler JJ, Allwood EG, Ayscough KR. WASP family proteins, more than Arp2/3 activators. Biochem Soc Trans. 2016;44:1339-45.

13. Espinoza-Sanchez S, Metskas LA, Chou SZ, Rhoades E, Pollard TD. Conformational changes in Arp2/3 complex induced by ATP, WASp-VCA, and actin filaments. Proceedings of the National Academy of Sciences. 2018;115(37):E8642.

14. Ti SC, Jurgenson CT, Nolen BJ, Pollard TD. Structural and biochemical characterization of two binding sites for nucleation-promoting factor WASp-VCA on Arp2/3 complex. Proc Natl Acad Sci U S A. 2011;108(33):E463-71.

15. Padrick SB, Doolittle LK, Brautigam CA, King DS, Rosen MK. Arp2/3 complex is bound and activated by two WASP proteins. Proceedings of the National Academy of Sciences. 2011;108(33):E472.

16. Yarar D, D'Alessio JA, Jeng RL, Welch MD. Motility determinants in WASP family proteins. Molecular Biology of the Cell. 2002;13(11):4045-59.

17. Rodal AA, Manning AL, Goode BL, Drubin DG. Negative regulation of yeast WASp by two SH3 domain-containing proteins. Curr Biol. 2003;13(12):1000-8.

18. Carlier MF, Nioche P, Broutin-L'Hermite I, Boujemaa R, Le Clainche C, Egile C, et al. GRB2 links signaling to actin assembly by enhancing interaction of neural Wiskott-Aldrich syndrome protein (N-WASp) with actin-related protein (ARP2/3) complex. J Biol Chem. 2000;275(29):21946-52.

19. Hoffman CS, Wood V, Fantes PA. An Ancient Yeast for Young Geneticists: A Primer on the Schizosaccharomyces pombe Model System. Genetics. 2015;201(2):403-+.

20. Goode BL, Eskin JA, Wendland B. Actin and Endocytosis in Budding Yeast. Genetics. 2015;199(2):315-58.

21. Weinberg J, Drubin DG. Clathrin-mediated endocytosis in budding yeast. Trends Cell Biol. 2012;22(1):1-13.

22. Lee WL, Bezanilla M, Pollard TD. Fission yeast myosin-I, Myo1p, stimulates actin assembly by Arp2/3 complex and shares functions with WASp. J Cell Biol. 2000;151(4):789-99.

23. MacLean-Fletcher S, Pollard TD. Identification of a factor in conventional muscle actin preparations which inhibits actin filament self-association. Biochem Biophys Res Commun. 1980;96(1):18-27.

24. Doolittle LK, Rosen MK, Padrick SB. Measurement and analysis of in vitro actin polymerization. Methods Mol Biol. 2013;1046:273-93.

25. Pollard TD. Rate constants for the reactions of ATP- and ADP-actin with the ends of actin filaments. Journal of Cell Biology. 1986;103(6):2747-54.

26. Doerfel LK, Wohlgemuth I, Kothe C, Peske F, Urlaub H, Rodnina MV. EF-P Is Essential for Rapid Synthesis of Proteins Containing Consecutive Proline Residues. Science. 2013;339(6115):85.

27. Ziemer MA, Mason A, Carlson DM. Cell-free translations of proline-rich protein mRNAs. Journal of Biological Chemistry. 1982;257(18):11176-80.

28. Pierce J, Suelter CH. An evaluation of the Coomassie brilliant blue G-250 dye-binding method for quantitative protein determination. Analytical Biochemistry. 1977;81(2):478-80.

29. Van Kley H, Hale SM. Assay for protein by dye binding. Analytical Biochemistry. 1977;81(2):485-7.

30. Allwood EG, Tyler JJ, Urbanek AN, Smaczynska-de R, II, Ayscough KR. Elucidating Key Motifs Required for Arp2/3-Dependent and Independent Actin Nucleation by Las17/WASP. PLoS One. 2016;11(9):e0163177.

31. Pollard TD. Measurement of rate constants for actin filament elongation in solution. Anal Biochem. 1983;134(2):406-12.

32. Horan BG, Zerze GH, Kim YC, Vavylonis D, Mittal J. Computational modeling highlights the role of the disordered Formin Homology 1 domain in profilin-actin transfer. FEBS Lett. 2018;592(11):1804-16.

33. Wu J-Q, Pollard TD. Counting Cytokinesis Proteins Globally and Locally in Fission Yeast. Science. 2005;310(5746):310.

34. Sirotkin V, Berro J, Macmillan K, Zhao L, Pollard TD. Quantitative analysis of the mechanism of endocytic actin patch assembly and disassembly in fission yeast. Mol Biol Cell. 2010;21(16):2894-904.

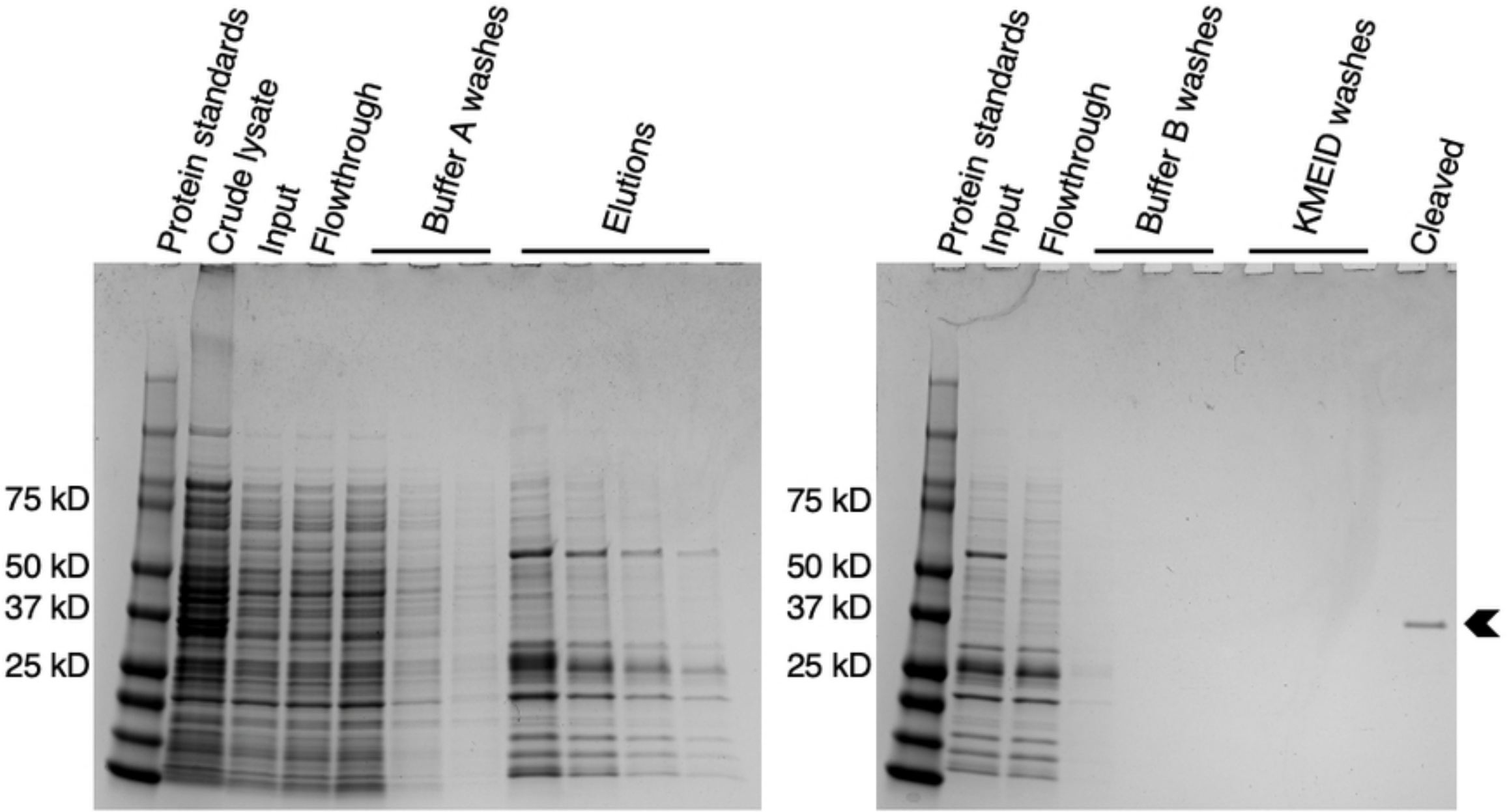
Protein standards
Crude lysate
Input
Flowthrough
Buffer A washes
Elutions
75 kD
50 kD
37 kD
25 kD
Protein standards
Input
Flowthrough
Buffer B washes
KMEID washes
Cleaved
75 kD
50 kD
37 kD
25 kD

Figure

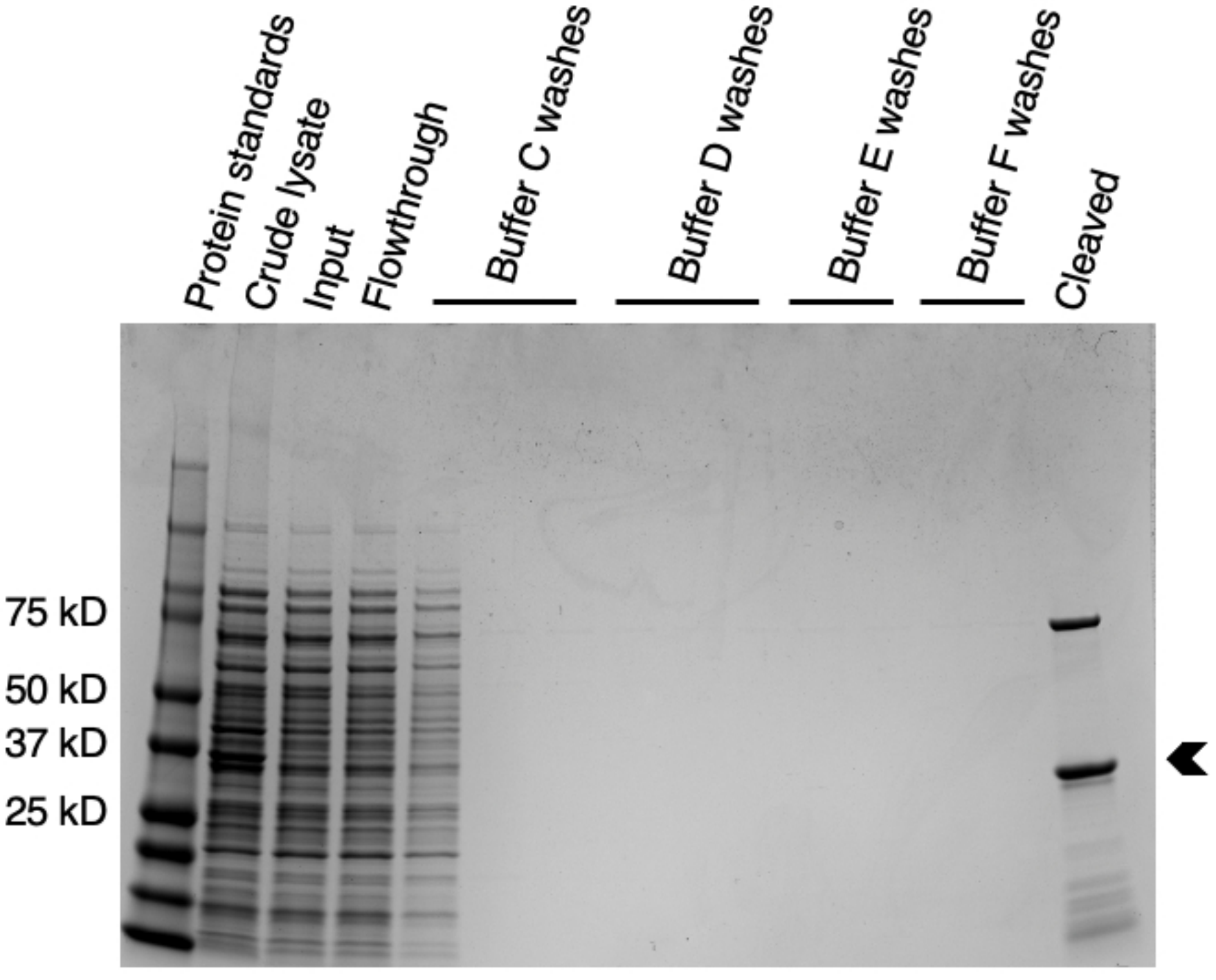
Protein standards
Crude lysate
Input
Flowthrough
Buffer C washes
Buffer D washes
Buffer E washes
Buffer F washes
Cleaved
75 kD
50 kD
37 kD
25 kD

Figure

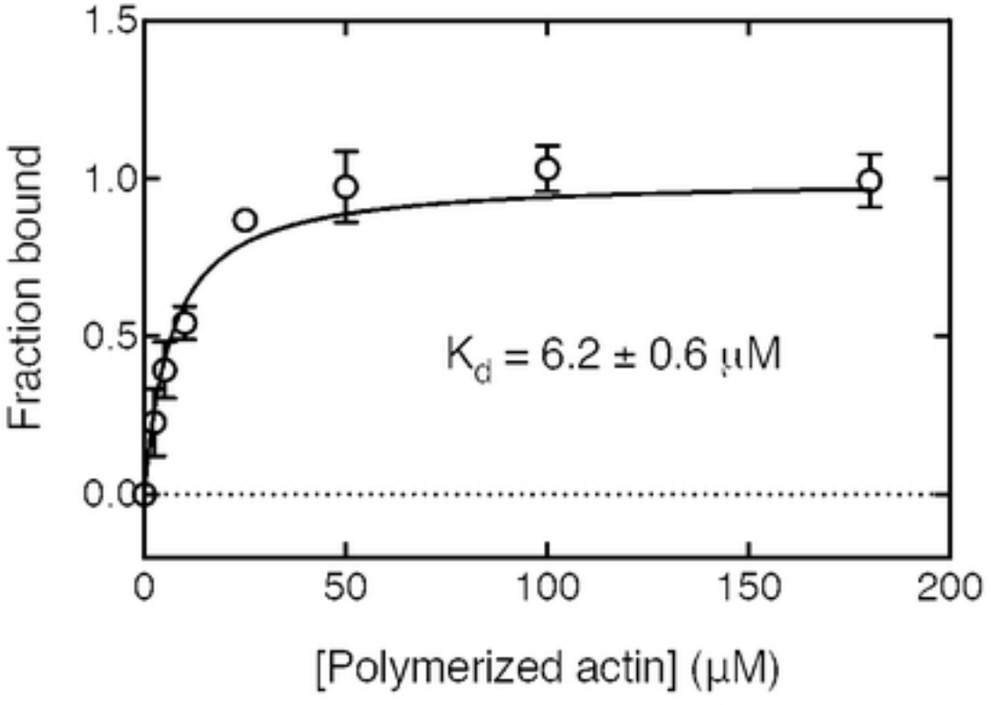
1.5
1.0
0.5
0.0
Fraction bound
K_d = 6.2 ± 0.6 μM
0
50
100
150
200
[Polymerized actin] (μM)

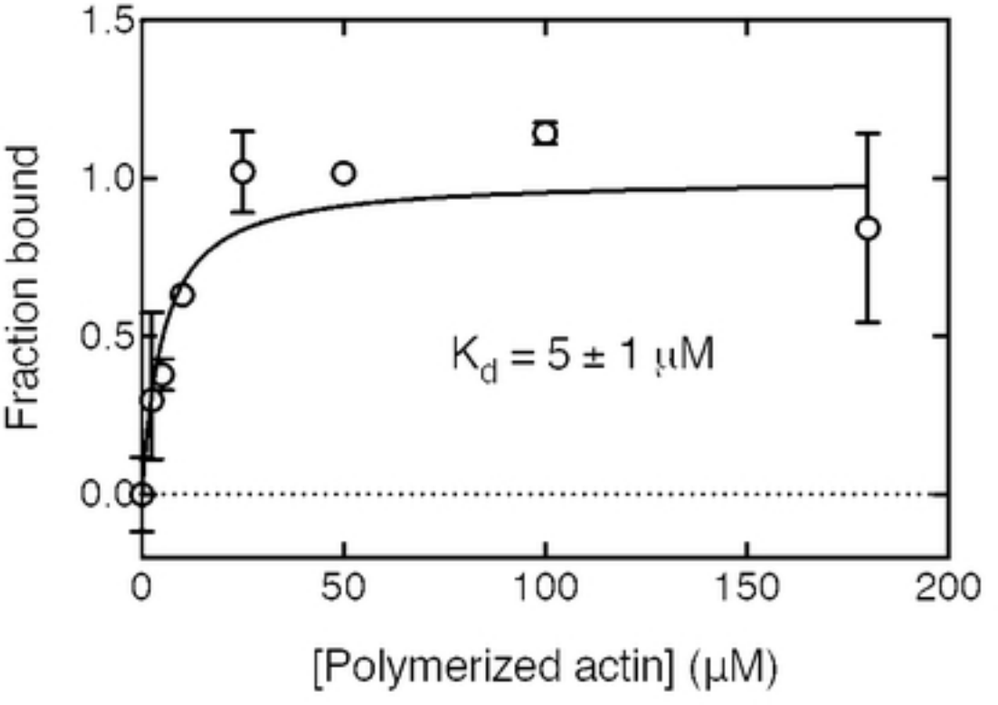
1.5
1.0
0.5
0.0
Fraction bound
K_d = 5 ± 1 μM
0
50
100
150
200
[Polymerized actin] (μM)

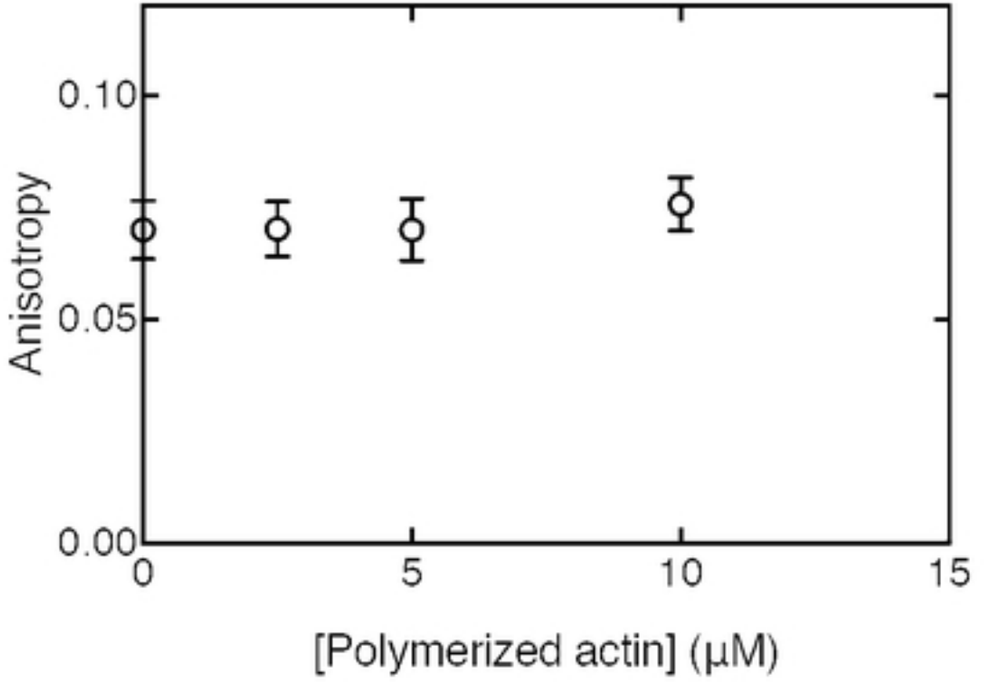
0.10
0.05
0.00
Anisotropy
0
5
10
15
[Polymerized actin] (μM)

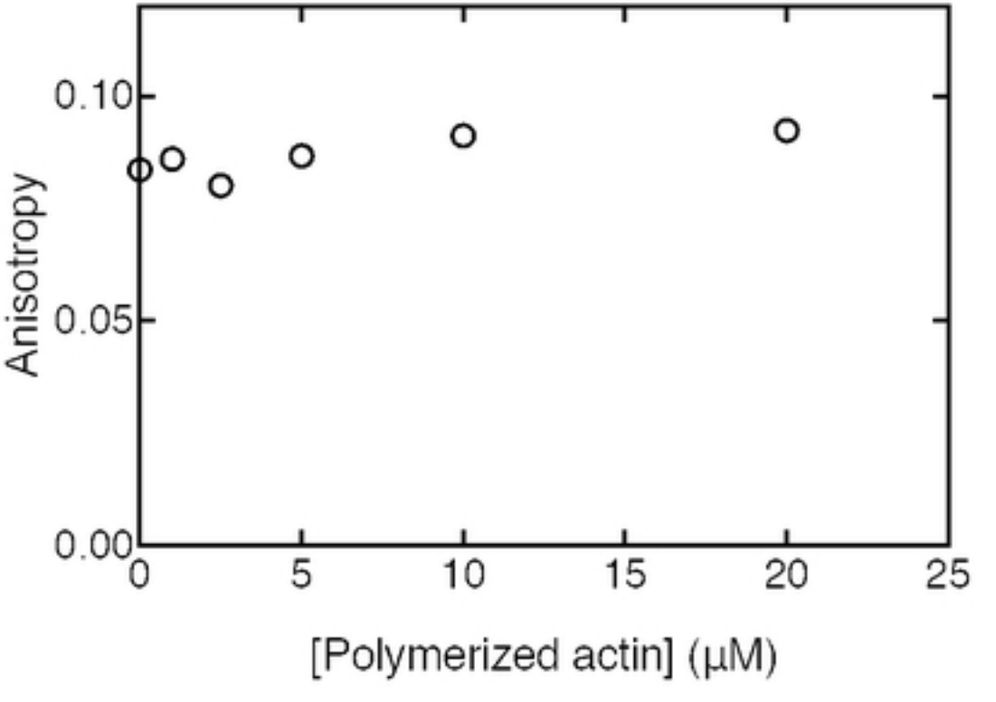
0.10
0.05
0.00
Anisotropy
0
5
10
15
20
25
[Polymerized actin] (μM)

Figure

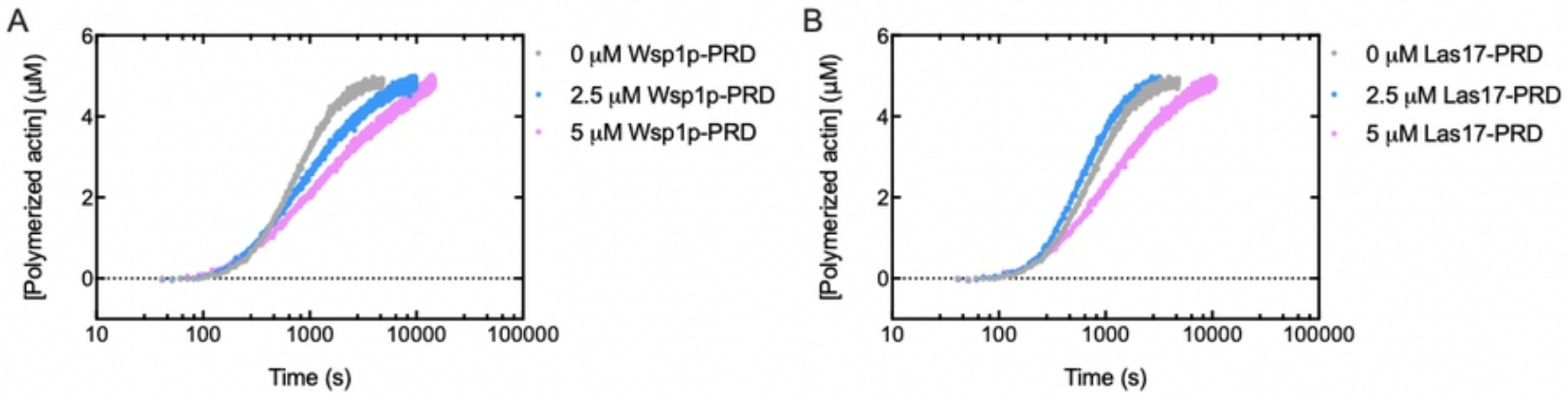
A
[Polymerized actin] (μM)
6
4
2
0
10
100
1000
10000
100000
Time (s)
0 μM Wsp1p-PRD
2.5 μM Wsp1p-PRD
5 μM Wsp1p-PRD
B
[Polymerized actin] (μM)
6
4
2
0
10
100
1000
10000
100000
Time (s)
0 μM Las17-PRD
2.5 μM Las17-PRD
5 μM Las17-PRD

Figure

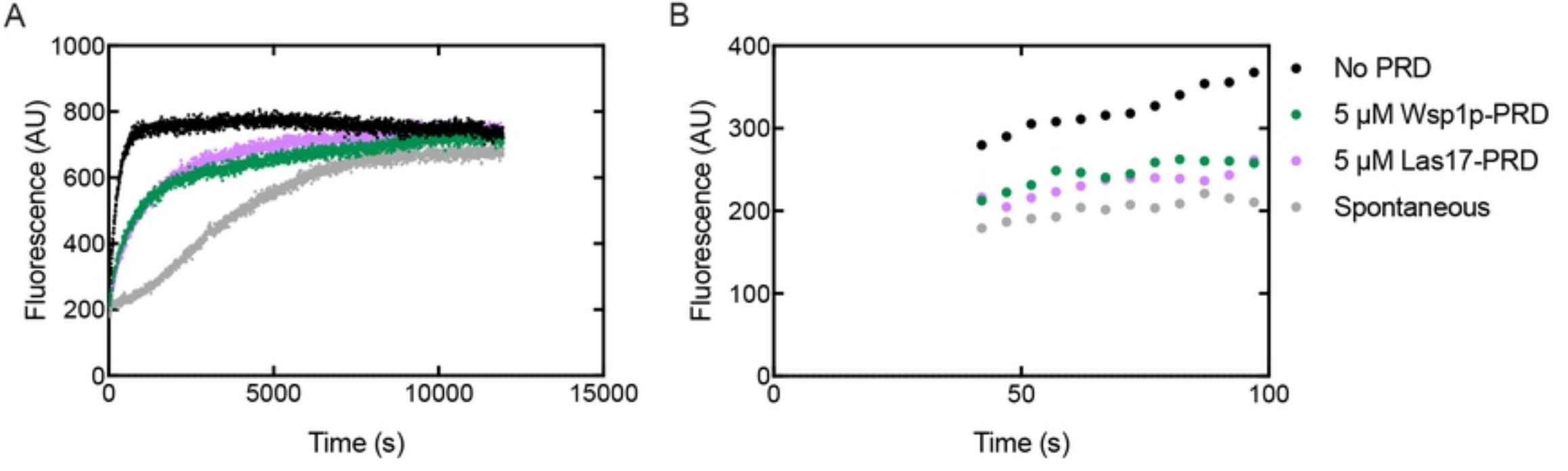
A
1000
800
600
400
200
0
Fluorescence (AU)
0
5000
10000
15000
Time (s)
B
400
300
200
100
0
Fluorescence (AU)
0
50
100
Time (s)
No PRD
5 μM Wsp1p-PRD
5 μM Las17-PRD
Spontaneous

Figure